Mon. Not. R. Astron. Soc. **000**, 000–000 (0000) Printed 27 October 2011 (MN LATEX style file v2.2)

Chemical signatures of formation processes in the stellar populations of simulated galaxies

Patricia B. Tissera[1,2], Simon D.M. White[2], Cecilia Scannapieco[3]
[1] *Instituto de Astronomía y Física del Espacio, Casilla de Correos 67, Suc. 28, 1428, Buenos Aires, Argentina. Conicet - UBA*
[2] *Max-Planck Institute for Astrophysics, Karl-Schwarzchild Str. 1, D85748, Garching, Germany*
[3] *Leibniz-Institute for Astrophysics Potsdam (AIP), An der Sternwarte 16, D-14482, Postdam, Germany*

27 October 2011

ABSTRACT
We study the chemical properties of the stellar populations in eight simulations of the formation of Milky-Way mass galaxies in a ΛCDM Universe. Our simulations include metal-dependent cooling and an explicitly multiphase treatment of the effects on the gas of cooling, enrichment and supernova feedback. We search for correlations between formation history and chemical abundance patterns. Differing contributions to spheroids and discs from *in situ* star formation and from accreted populations are reflected in differing chemical properties. Discs have younger stellar populations, with most stars forming *in situ* and with low α-enhancement from gas which never participated in a galactic outflow. Up to 15 per cent of disc stars can come from accreted satellites. These tend to be α-enhanced, older and to have larger velocity dispersions than the *in situ* population. Inner spheroids have old, metal-rich and α-enhanced stars which formed primarily *in situ*, more than 40 per cent from material recycled through earlier galactic winds. Few accreted stars are found in the inner spheroid unless a major merger occurred recently. Such stars are older, more metal-poor and more α-enhanced than the *in situ* population. Stellar haloes tend to have low metallicity and high α-enhancement. The outer haloes are made primarily of accreted stars. Their mean metallicity and α-enhancement reflect the masses of the disrupted satellites where they formed: more massive satellites typically have higher [Fe/H] and lower [α/Fe]. Surviving satellites have distinctive chemical patterns which reflect their extended, bursty star formation histories. These produce lower α-enhancement at given metallicity than in the main galaxy, in agreement with observed trends in the Milky Way.

Key words: galaxies: formation, galaxies: evolution, galaxy:stellar content, cosmology: theory

1 INTRODUCTION

According to the current cosmological paradigm, galaxy formation occurred through the condensation of gas in the cores of a hierarchically growing population of dark haloes. This strongly nonlinear process can be followed in detail only with sophisticated numerical simulations. Advances in numerical techniques and in computational power, together with the accumulation of more precise and more detailed observations of the galaxy population, have enabled substantional improvements in our understanding of cosmic structure formation. Nevertheless important open questions remain, in particular on galactic scales (Mo et al. 2010). Many of these issues are related to the evolution of the baryons. A variety of physical processes, acting on different scales and with differing efficiency, are believed to play a role in determining the properties of galaxies. Direct simulation of galaxy formation in a ΛCDM context has evolved greatly in recent years (e.g. Springel 2005; Scannapieco et al. 2006; Governato et al. 2007; Brook et al. 2007; Stinson et al. 2006; Sijacki et al. 2007; Scannapieco et al. 2009; Agertz et al. 2009; Schaye et al. 2010; Agertz et al. 2011; Brook et al. 2011) with improved descriptions of cooling, star formation, black hole formation, and luminous, mechanical and material feedback from star-forming regions and active galactic nuclei. Nevertheless, most aspects of this critical baryonic physics are still described by schematic, phenomenological sub-grid models, since it is not yet possible to achieve the small-scale resolution needed to simulate them *ab initio*.

Confronting such simulations with observation is a key route to improving the models and developing a better

understanding of galaxy growth in its cosmological context. Chemical patterns can be powerful tools for advancing this programme. The elements are synthesized in stars and ejected into the interstellar medium (ISM) through stellar winds and supernovae (SNe). Different SN types release their nucleosynthesis products on different timescales, imprinting characteristic chemical patterns on the stellar populations which form from the gas they enrich (as observed in the Milky Way, see e.g Bland-Hawthorn & Freeman 2003; Wyse 2010). SN products are mixed with other interstellar gas by internal mechanisms, or may even be thrown out of the galaxy as part of a wind. Environmental effects such as interactions with other galaxies or ram pressure stripping as a result of motion through the intergalactic medium, also play a role by mixing new heavy elements into the intergalactic medium. Galaxy mergers induce major starbursts which substantially modify the abundance patterns in the ISM (e.g. Perez et al. 2006; Di Matteo et al. 2009; Rupke et al. 2010, Perez et al. submitted). Even minor mergers with infalling satellites modify metal abundance patterns by contributing stars and gas with distinctive abundances and by triggering new star formation activity (e.g. Barnes & Hernquist 1996; Mihos & Hernquist 1996; Tissera 2000).

The possible contribution of disrupted satellites to the stellar populations of thin discs (Abadi et al. 2003), thick discs (Huang & Carlberg 1997) and bulges (Rahimi et al. 2010) has been much debated. Some simulations have suggested that stellar haloes may have formed primarily through satellite disruption (e.g. Johnston et al. 2008; Cooper et al. 2010), but there have also been claims for a dual formation route, depending on the early merging history of each individual galaxy (e.g. Zolotov et al. 2009, 2010); this may be supported by abundance patterns in the stellar halo and satellites of the Milky Way (Venn et al. 2004). Different evolutionary paths are expected to leave their fingerprints on the chemical and dynamical properties of the stellar populations, and analysing such fingerprints should help us to learn more about how galaxies formed.

Much work has been devoted to understanding if chemical patterns can indeed be related to specific events during galaxy formation (e.g. Mollá & Ferrini 1995; Chiappini et al. 1997). Within the current hierarchical paradigm, the nonlinearity and complexity of structure growth require chemical and structural evolution to be treated simultaneously and consistently if reliable conclusions are to be drawn. In the last decade a variety of treatments of chemical evolution have been implemented in the cosmological hydrodynamics codes used to simulate galaxy formation (e.g. Raiteri et al. 1996; Mosconi et al. 2001; Lia et al. 2002; Kawata & Gibson 2003; Kobayashi et al. 2007; Wiersma et al. 2009; Martínez-Serrano et al. 2008). These typically adopt the standard metal production assumptions from analytic models of chemical evolution (e.g. Tinsley & Larson 1979; Matteucci & Greggio 1986) but follow the formation and transport of elements among the various components of the system in a dynamically consistent way. Such codes have already given a number of encouraging results, reproducing general trends observed in the galaxy population such as the mass-metallicity relation, for example (Governato et al. 2007; Kobayashi et al. 2007).

The simulations analysed in the current paper follow the formation of galaxies within a set of eight Milky-Way-mass haloes from the Aquarius Project (Springel et al. 2008). The resulting central galaxies have been extensively studied in papers by Scannapieco et al. (2009), Tissera et al. (2010), Scannapieco et al. (2010) and Scannapieco et al. (2011). These studies highlighted the difficulty in forming spirals similar to the Milky Way within the ΛCDM cosmology (but see Guedes et al. (2011) who were able to produce an L^* disk galaxy with a low i-band bulge-to-disk ratio in a single high-resolution simulation which assumed a higher surface density threshold for star formation than earlier simulations like our own.). Scannapieco et al. (2009) found that although most of the simulated galaxies had a substantial disc at some stage during their evolution, these discs are often disrupted by interactions with satellites or destabilized by misaligned inflowing cold gas. These processes feed the growth of stellar spheroids, which end up as the dominant components by mass in all the simulations. Thus, at $z = 0$ none of our simulated haloes hosts a spiral with a disc-to-total mass ratio similar to that of the Milky Way. In spite of this, the final discs and spheroids show general dynamical properties which are quite consistent with those of observed spiral galaxies. While the spheroids are dominated by old, dynamically hot stars (and tend to rotate more slowly than observed bulges), the discs have the youngest stars, they formed typically from the inside out, and they are dynamically cold. Residual cold gas forms a well-behaved disc in equilibrium within its potential well (Scannapieco et al. 2011). The fact that these two components show distinct star formation histories and distinct dynamical properties prompted us to explore their chemical properties, seeking chemical signatures which can be related to specific details of their formation histories.

The simulations studied here use a specially enhanced version of GADGET-3 which is itself an optimisation of GADGET-2 (Springel 2005). Our version includes a chemical and energy feedback model which is consistently coupled to a unique multiphase representation of the interstellar medium (ISM) which allows collocation, material exchange, and relative motion between the different phases. This scheme allows us to follow the dynamical and chemical properties of baryons throughout the galaxy formation process. Dense and cold gas is transformed into stars which can explode as SN. These inject entropy into some of the remaining cold gas, converting it to the hot diffuse phase and driving powerful, mass-loaded winds. These thermodynamic changes are generated on a particle-by-particle basis in a way which is consistent with local astrophysical conditions. As a result star-forming regions drive winds without the need to temporarily suspend cooling, to impart large kicks to particles, or to suppress hydrodynamical interactions with surrounding particles. This naturally results in self-regulated winds which are adapted to the depth of the potential well in which star formation is occurring (Scannapieco et al. 2006, 2009; Sawala et al. 2010, 2011; De Rossi et al. 2010). In this framework, gas is progressively enriched as subsequent stellar generations release new elements into the ISM, so that the chemical structure of each galaxy is intimately related to the formation paths of its various components. In this paper, we focus on this relation between chemical properties and assembly history. In a subsequent paper, we will analyse how gas flows lead to abundance gradients (Tissera et al. 2011 in preparation).

In Section 2 we describe our simulations and the main

aspects of our chemical model. We also include a subsection explaining the criteria we adopt to separate our galaxies into their dynamical components. In Section 3 we study the chemical properties of these components, together with their formation histories. Section 4 studies the chemical properties of stars formed *in situ* and contrasts them with those of stars accreted from tidally disrupted satellites. Section 5 compares the mean chemical abundances of stars from disrupted satellites with those of stars in surviving satellites. We summarize our findings in the concluding section.

2 THE SIMULATIONS

We have analysed galaxy formation within a set of eight haloes selected and simulated at high resolution as part of the Aquarius Project (Springel et al. 2008). These objects were identified in a lower-resolution version of the Millennium-II Simulation (Boylan-Kolchin et al. 2009), a cosmological simulation of a cubic region 100 Mpc h^{-1} on a side, imposing a mild isolation criterion and requiring a mass similar to that of the Milky Way's halo at $z = 0$. In the original project these haloes were simulated at a variety of resolutions following the dark matter only. For the simulations discussed here, gas particles were added to the initial conditions on a cubic mesh displaced by half the interparticle separation from the dark matter particle mesh. Details can be found in Scannapieco et al. (2009).

All these simulations assumed a ΛCDM cosmogony with $\Omega_{\rm m} = 0.25, \Omega_\Lambda = 0.75, \Omega_{\rm b} = 0.04, \sigma_8 = 0.9, n_s = 1$ and $H_0 = 100\ h\ \mathrm{kms}^{-1}\mathrm{Mpc}^{-1}$ with $h = 0.73$. Our galaxy formation simulations were carried out with maximum gravitational softenings in the range $\epsilon_G = 0.5 - 1$ kpc h^{-1}, dark matter particle masses of order $10^6 \mathrm{M}_\odot h^{-1}$ and initial gas particle masses of order $2 \times 10^5 \mathrm{M}_\odot h^{-1}$. Since their virial masses are in the range 5 to $11 \times 10^{11} \mathrm{M}_\odot h^{-1}$, the final systems all have about a million particles in total within the virial radius[1]. In Table 2 we summarize their principal characteristics. Our naming convention (Aq-A-5, etc.) follows that of earlier papers. The capital letter (A to H) designates the particular halo considered, whereas the number (1 to 5) indicates the resolution level of the simulation according to the original Aquarius convention. All simulations studied in this paper are at level 5 the lowest of the original Aquarius resolutions. Further details can be found in Scannapieco et al. (2009).

Scannapieco et al. (2009) and Scannapieco et al. (2011) studied the formation of the disc and the spheroidal components of these systems and their dynamical and photometric properties, while Tissera et al. (2010) analysed the reponse of their dark matter haloes to the galaxy formation process. The main galaxies have a variety of morphologies with varying bulge-to-disc ratios and strong bars in several cases. Nevertheless, all of them are bulge dominated, and one (Aq-F-5) has no detectable disc at all at $z = 0$. In this paper, we focus on the chemical properties and the assembly histories of the various stellar components of the galaxies.

[1] We define the virial radius (r_{200}) as the radius within which the mean mass density of all components is 200 times the critical value. The virial mass is then the total mass within this radius.

2.1 The galaxy formation simulation code

The version of GADGET-3 used to carry out these simulations has been extended to include an explicit multiphase model for the gas component which allows a cold, dense, possibly star-forming phase and a hot, diffuse phase to interpenetrate, to move relative to each other, and to exchange material. This implementation also includes metal-dependent cooling, star formation, and chemical and thermal feedback into both gas phases. as described in Scannapieco et al. (2005) and Scannapieco et al. (2006). This scheme has been successful in reproducing the star formation activity of galaxies during both quiescent and starburst phases, and can drive substantial mass-loaded galactic winds from star-forming galaxies with a wide range of masses at speeds that consistently reflect the depth of the individual potential wells (Scannapieco et al. 2006, 2008; Sawala et al. 2010, 2011; De Rossi et al. 2010). The scheme does not require any *ad hoc* "fixes" (for example, temporary suppression of radiative cooling and/or of hydrodynamic coupling for wind particles, or the imposition of discontinuous momentum changes to "kick-start" a wind) to ensure efficient wind generation in SPH simulations, and there are no scale-dependent parameters. As a result, it is particularly well suited for the study of galaxy formation in a cosmological context where galaxies with a wide range of properties form simultaneously. The version used here includes chemical enrichment by Type II and Type Ia supernovae (SNII and SNIa, respectively) as we describe next.

2.1.1 The Chemical Model

The chemical evolution model adopted in this work is that developed by Mosconi et al. (2001) and adapted by Scannapieco et al. (2009) to GADGET-3. We consider chemical elements which are synthesised in stellar interiors and then ejected into the ISM by SNII and SNIa events. A Salpeter Initial Mass Function is assumed with lower and upper mass cut-offs at 0.1 $\mathrm{M}_\odot$ and 40 $\mathrm{M}_\odot$, respectively. We follow 12 different chemical isotopes: H, ^{4}He, ^{12}C, ^{16}O, ^{24}Mg, ^{28}Si, ^{56}Fe, ^{14}N, ^{20}Ne, ^{32}S, ^{40}Ca and ^{62}Zn. Initially, all baryons are in the form of gas with primordial abundances, i.e. 76% H and 24% ^{4}He by mass.

SNII are considered to originate from stars more massive than 8 $\mathrm{M}_\odot$, adopting the metal-dependent yields of Woosley & Weaver (1995). We use the metal-and-mass dependent lifetimes given by the fitting formulae of Raiteri et al. (1996). For SNIa, we adopt the W7 model of Thielemann et al. (1993) which assumes that SNIa events originate from CO white dwarf systems in which mass is transferred from the secondary to the primary star until the Chandrasekhar mass is exceeded and an explosion is triggered. For simplicity, we assume that the lifetime of the progenitor systems is distributed uniformly and at random over the range $[0.7, 2]$ Gyr. To calculate the number of SNIa, we adopt an observationally motivated rate of 0.3 relative to SNII (Mosconi et al. 2001).

The ejection of chemical elements is grafted onto the SN feedback model so that chemical elements are distributed to the cold and the hot gas phases surrounding a given star particle. The fraction of elements going to each phase is regulated by a free parameter $\epsilon_{\rm c}$ which also determines the

amount of SN energy received by each phase. While the injection of energy follows two different paths depending on the thermodynamical properties of the gas, chemical elements are added to both phases at the time each SN occurs. All the simulations of this paper have been run with $\epsilon_c = 0.5$. Some tests of the effect of varying this parameter can be found in Scannapieco et al. (2006).

2.2 The stellar components of the simulated galaxies

As shown by Scannapieco et al. (2009), the simulated galaxies have a variety of morphologies and contain both spheroidal and disc components. Our main contribution to understanding how these galaxies formed comes from linking their dynamical evolution with specific chemical patterns in their stellar populations.

Several methods for separating spheroids and discs have been proposed (e.g. Abadi et al. 2003; Governato et al. 2009; Scannapieco et al. 2009). In this work we use a procedure similar to that of Abadi et al. (2003). We measure $\epsilon = J_z/J_{z,\rm max}(E)$ for each star, where J_z is the angular momentum component perpendicular to the disc plane and $J_{z,\rm max}(E)$ is the maximum J_z over all particles of given total energy, E. A star on a prograde circular orbit in the disc plane has $\epsilon \simeq 1$. In Fig. 1 we show ϵ as a function of total energy for the stars in each of the Aquarius haloes. The colour code indicates stellar metallicity, [Fe/H]. Discs are easily identified as star concentrations near $\epsilon = 1$ while stars in the spheroidal components usually scatter around $\epsilon = 0$. The bulge is located at the lowest (most bound) energies, while the outer halo is at the highest (least bound) energies.

We define stars to belong to different dynamical components according to their location in Fig.1. We consider stars with $\epsilon > 0.65$ to be part of a disc. This value is small enough to include stars in both thin and thick discs. Particles which do not satisfy this requirement are taken to be part of the spheroid. Motivated by observations of the Milky Way spheroid which report differences in stellar kinematics and chemical abundances as one moves outwards (Carollo et al. 2007; Zoccali et al. 2008), we separate our spheroids into three subregions according to their binding energy. The central spheroid ("bulge") is defined to consist of stars more bound than the minimum energy ($E_{\rm cen}$) of stars with $r \geq 0.5 \times r_{\rm opt}$ where the characteristic radius $r_{\rm opt}$ is defined to enclose 83% of the baryonic mass of the simulated galaxy. Central spheroid stars thus all have orbital apocentres less than about $0.5r_{\rm opt}$. Stars more weakly bound than $E_{\rm cen}$ but with $E < E_{\rm inner}$, the minimum energy of all stars with $r > 2 \times r_{\rm opt}$ are considered to form the inner halo. Stars with $E > E_{\rm inner}$ are defined to belong to the outer halo and thus all have orbital pericentres outside about $2r_{\rm opt}$. Although there is some arbitrariness in these criteria, the main features of the components change only slowly with the reference energies. Our criteria are chosen so that the definition of the spheroidal components adapts to the overall size of each individual galaxy. Fig. 1 indicates the two bounding energies($E_{\rm cen}$ and $E_{\rm inner}$) for each Aquarius system.

The disks extend over a relatively small range of energies and thus radii in Aq-A and B, but over a more substantial range in Aq-C, D, E and G. Aq-F and H appear to have very little disc at all. The relative mass of the discs is seen more easily in Fig.2 where we give histograms of ϵ for all stars within $2r_{\rm opt}$ in each of our galaxies. Returning to Fig1, the central spheroid is seen to have rather little rotation in Aq-A, C, D, F, G and H, but is clearly rotating in the same sense as the disc in Aq-E. In Aq-B the inner spheroid is rotating in the same sense as the disc in the innermost regions but in the opposite sense at intermediate energies.

The inner stellar halo is essentially non-rotating in all cases except Aq-E and F. In the former there is no clear separation of the inner halo and disk populations, as is particularly evident in Fig.2. The outer halo is non-rotating in all cases except Aq-F, and in most galaxiees it shows stellar concentrations associated with satellite galaxies and stellar streams (i.e. disrupted satellites). For our main analysis we remove all satellites detected as individual bound structures in order to focus on the "diffuse" stellar halo. The chemical abundances of surviving satellites are analysed separately in the last section of this paper. Colour variations between components in different panels of Fig.1 indicate different levels of chemical enrichment. In general, strongly bound stellar populations are more chemically enriched than those found at lower energies. However, disc stars are clearly more chemically enriched than spheroid stars of similar energy.

3 FORMATION HISTORIES OF THE STELLAR COMPONENTS AND THEIR GLOBAL CHEMICAL PROPERTIES

It has long been suggested that particular chemical patterns are linked to key events in the formation history of galaxies. In this section, we will address this question by comparing formation history with $z = 0$ abundance pattern for the various components of our galaxies.

In Fig. 3, we present star formation histories for individual stellar components in the form of cumulative plots of the fraction of the final stellar mass formed as a function of age. In such plots, a step reflects a starburst. The central spheroid and the inner and outer haloes have quite similar SF histories, with most of their stars formed at very high redshift. The oldest stars are split between the central spheroid and the haloes. The discs contain younger stellar populations which form in a series of episodes spread over the Hubble time. In the case of Aq-F-5, no disc component survives at $z = 0$.

Star formation histories vary from system to system as a consequence of differing evolutionary paths, leading to variations in chemical properties between our galaxies and between components within a galaxy. This can be seen in Fig. 4 where we show [Fe/H] distributions for the individual stellar components in four of our simulated haloes. Interestingly, while the central spheroids, the inner and the outer stellar haloes all have similar star formation histories (see Fig. 3) their [Fe/H] distributions are very different. Comparing individual stellar components between galaxies, we also note significant variations in the abundance distributions.

The relative abundance of α-elements with respect to Fe is often identified as a key property to characterise the formation histories of stellar populations. We have measured [O/Fe] distributions for the individual stellar components in

Table 1. General characteristics of our main galaxies and their haloes at $z = 0$. The left column shows the halo name. r_{200} and M_{200} are the virial radius and mass, respectively. $N_{\rm dm}$, $N_{\rm gas}$, $N_{\rm hot}$ and N_* are the total numbers of dark matter, gas, hot gas and star particles within r_{200}, respectively. $r_{\rm opt}$ is the optical radius of the galaxy and $M_*^{\rm opt}$ and $N_*^{\rm opt}$ are the stellar mass and the number of star particles estimated within twice $r_{\rm opt}$.

Halo	r_{200} h^{-1}kpc	M_{200} $10^{12}h^{-1}{\rm M}_\odot$	$M_{\rm hot}$ $10^{10}h^{-1}{\rm M}_\odot$	$M_{\rm cold}$ $10^{10}h^{-1}{\rm M}_\odot$	$N_{\rm dm}$	$N_{\rm gas}$	$N_{\rm hot}$	N_*	$r_{\rm opt}$ ${\rm h}^{-1}$kpc	$M_*^{\rm opt}$ $10^{10}h^{-1}{\rm M}_\odot$	$N_*^{\rm opt}$
Aq-A-5	169.42	1.10	4.1	1.1	529110	92159	72157	333409	13.1	5.92	277382
Aq-B-5	132.10	0.52	1.2	0.6	435330	63580	41312	291313	13.0	2.53	244511
Aq-C-5	173.19	1.18	3.4	0.6	681143	97796	83845	548964	11.7	5.93	432232
Aq-D-5	170.63	1.09	1.7	0.2	599438	82736	75741	377866	10.8	4.41	287734
Aq-E-5	149.93	0.79	2.1	0.6	554245	80524	63458	512809	10.1	4.97	406399
Aq-F-5	142.74	0.67	1.6	0.2	680129	79345	71124	699052	10.3	5.39	525101
Aq-G-5	142.64	0.68	1.2	0.5	679177	74675	52828	387751	10.3	5.63	334108
Aq-H-5	132.94	0.53	0.5	0.1	515392	23133	20671	546482	7.60	4.73	425680

Table 2. Properties of the stellar components of the main galaxies at $z = 0$. $M_{\rm disc}$, $M_{\rm cen}$, $M_{\rm Inner}$ and $M_{\rm Outer}$ are the stellar masses of disc, central spheroid, inner halo and outer halo of the main Aquarius galaxies as obtained from the kinematic decomposition. All masses are given in units of $10^9h^{-1}{\rm M}_\odot$. D/T^1 and D/T^2 are the disc-to-total stellar mass considering as total mass only the stellar discs and the central spheroids (T^1) and also the stellar inner haloes (T^2). The last column show ${\rm D/T^{photo}}$ photometric ratios calculated by Scannapieco et al. (2010) using an observationally based approach (for Aq-F-5 amd Aq-H-5, they could not obtain a reliable photometric decomposition).

Halo	$M_{\rm disc}$	$M_{\rm cen}$	$M_{\rm Inner}$	$M_{\rm Outer}$	${\rm D/T^1}$	${\rm D/T^2}$	${\rm D/T^{photo}}$
Aq-A-5	3.2	3.4	14.6	2.4	0.08	0.06	0.32
Aq-B-5	2.2	16.9	6.4	1.4	0.11	0.09	0.42
Aq-C-5	1.6	37.8	14.2	3.6	0.29	0.23	0.49
Aq-D-5	8.9	24.0	13.6	4.0	0.27	0.19	0.68
Aq-E-5	1.1	25.2	15.3	2.1	0.30	0.21	0.40
Aq-F-5	-	39.0	9.5	0.5	—	—	—
Aq-G-5	6.0	16.0	7.3	0.7	0.27	0.20	0.60
Aq-H-5	1.3	15.6	22.3	2.5	0.07	0.03	—

four of our galaxies as displayed in Fig. 4 (upper raw). As in the Milky Way, discs show the lowest level of α-enhancement. This is because their stars are younger than the other simulated stellar populations and formed over an extended period of time. As a result, the gas from which they formed had time to be enriched by SNIa. Stars in the central spheroids are α-enhanced but have the highest [Fe/H] values of all the populations, reflecting the fact that they formed in a short and strong starburst and were able to retain a large fraction of their SN ejecta. These general properties are in agreement with data for the Milky-Way bulge (Zoccali et al. 2008). The largest α-enhancements in our models are, however, found in the inner and outer stellar haloes.

Although the typical [Fe/H] values found for our bulge and disc components are lower than for their Milky Way counterparts, the trends between components are similar to those observed. There are clear variations between the various Aquarius galaxies, both in [Fe/H] and in α-enhancement, but the above mentioned trends seem to be common to all of them. Remaining differences with the Milky Way (for example the G-dwarf problem evident in Fig. 4) must, at least in part, be due to the fact that all the Aquarius galaxies have disc-to-spheroid mass ratios much smaller than that of the Milky Way. We also note that the metallicity distributions have large standard deviations which might suggest the need for more efficient metal mixing (Martínez-Serrano et al. 2008; Wiersma et al. 2009). For the discs and inner haloes, these large dispersions make it difficult to distinguish chemical differences. Nevertheless, for the best discs, Aq-C-5, Aq-D-5 and Aq-G-5, a Kolmogorov-Smirnov test shows the metallicity distributions of the discs and inner haloes to differ at confidence levels between 70 and 94 percent. Only for Aq-B-5 and Aq-H-5 do the the metallicity distributions of these components appear indistinguishable. In general, for all our galaxies, the spheroidal components show a decrease of [Fe/H] as one moves outwards. Their stellar populations are more α-enriched and older than those populating the corresponding disc components. Stars in the haloes are, on average, more α-enriched than those in the central spheroids.

To test how numerical resolution affects our estimates of chemical abundances, we have analysed two lower resolution versions of Aq-E which we label Aq-E-6 and Aq-E-7 [2]. Within r_{200} these have totals of about 160,000 and 80,000 particles, respectively, whereas Aq-E-5 has more than one million. These two lower resolution simulations were also analysed by. Scannapieco et al. (2009, 2011) and Tissera et al. (2010) who reported good agreement between their dynamical and structural properties and those of Aq-E-5,

[2] Simulations Aq-E-6 and Aq-E-7 correspond to those labeled as Aq-E-6b and Aq-E-6 in Scannapieco et al. (2011)

Table 3. Chemical properties of the stellar discs. The first column gives the encoding name of the halo. $F_{\rm prog}$ and $F_{\rm prom}$ are the fractions of stars formed in the progenitor systems and of stars which have been part of a galactic wind. σ/V is the ratio of velocity dispersion to mean circular velocity. Age is the mean stellar age in Gyr. [Fe/H] and [O/Fe] are median logarithmic abundances relative to solar. Standard deviations are included within parentheses. The superscripts "prog" and "sat" denote values corresponding to stars formed *in situ* and to stars acquired from disrupted satellites, respectively.

Halo	$F_{\rm prog}$	$F_{\rm prom}$	$\sigma/V^{\rm prog}$	$(\sigma/V)^{\rm sat}$	[Fe/H]$^{\rm prog}$	[Fe/H]$^{\rm sat}$	[O/Fe]$^{\rm prog}$	[O/Fe]$^{\rm sat}$	Age$^{\rm prog}$	Age$^{\rm sat}$
Aq-A-5	0.97	0.08	0.86	1.13	-1.10(0.43)	-1.75(1.35)	-0.163(0.133)	0.343(0.052)	5.89(7.53)	12.66(0.13)
Aq-B-5	0.91	0.09	0.67	0.89	-1.25 (0.62)	-1.55(1.03)	-0.174(0.154)	0.094(0.288)	4.08(4.19)	10.63(4.92)
Aq-C-5	0.99	0.09	0.59	0.76	-0.86 (0.33)	-1.37(0.81)	-0.131(0.121)	0.300(0.113)	8.69(5.07)	12.39(3.07)
Aq-D-5	0.89	0.15	0.68	0.77	-0.85 (0.34)	-0.97(0.73)	-0.096(0.114)	0.192(0.142)	7.99(6.47)	10.81(1.26)
Aq-E-5	0.62	0.30	0.54	0.60	-0.95 (0.36)	-0.83(0.58)	-0.049(0.123)	0.031(0.154)	8.53(2.98)	11.09(0.79)
Aq-F-5	—	—	—	—	—	—	—	—	—	—
Aq-G-5	0.97	0.12	0.62	0.73	-0.94(0.38)	-1.75(1.21)	-0.092(0.109)	0.076(0.259)	8.06(7.07)	12.22(2.85)
Aq-H-5	0.84	0.21	1.08	1.02	-0.90(0.39)	-1.25(1.08)	-0.137(0.131)	0.241(0.151)	7.72(7.03)	12.36(0.59)

Table 4. Chemical properties of the central spheroids. The first column gives the encoding name of the halo. $F_{\rm prog}$ and $F_{\rm prom}$ are the fractions of stars formed in the progenitor systems and of stars which have been part of a galactic wind. σ is the mean velocity dispersion (in km s^{-1}), while Age is the mean stellar age (in Gyr). [Fe/H] and [O/Fe] are median logarithmic abundances relative to solar. Standard deviations are included within parentheses. The superscripts "prog" and "sat" label values corresponding to stars formed *in situ* and to stars acquired from disrupted satellites, respectively.

Halo	$F_{\rm prog}$	$F_{\rm prom}$	[Fe/H]$^{\rm prog}$	[Fe/H]$^{\rm sat}$	[O/Fe]	[O/Fe]$^{\rm sat}$	Age$^{\rm prog}$	Age$^{\rm sat}$
Aq-A-5	0.96	0.43	-0.61(0.25)	-1.20(0.83)	0.023(0.126)	0.358(0.016)	11.46(1.67)	12.63(0.09)
Aq-B-5	0.79	0.64	-0.66(0.36)	-0.92(0.55)	-0.025(0.111)	0.159(0.092)	9.43(1.52)	10.93(1.56)
Aq-C-5	0.95	0.44	-0.61(0.34)	-1.12(0.56)	0.038(0.122)	0.353(0.033)	11.82(1.18)	12.52(0.04)
Aq-D-5	0.90	0.60	-0.62(0.29)	-0.99(0.63)	-0.003(0.110)	0.214(0.084)	10.75(1.39)	11.95(0.20)
Aq-E-5	0.71	0.75	-0.40(0.31)	-0.57(0.41)	-0.031(0.108)	0.014(0.109)	10.56(3.95)	11.53(0.65)
Aq-F-5	0.55	0.53	-0.52(0.32)	-0.65(0.50)	-0.061(0.103)	0.037(0.118)	10.58(4.62)	10.93(3.02)
Aq-G-5	0.74	0.73	-0.58(0.35)	-0.70(0.50)	0.048(0.112)	0.122(0.085)	11.37(2.00)	11.08(1.53)
Aq-H-5	0.83	0.78	-0.40(0.33)	-0.90(0.46)	-0.026(0.122)	0.358(0.028)	11.62(1.51)	12.45(0.09)

both for baryons and for dark matter. We find similarly good convergence for the chemical properties of each of our stellar components, as can be appreciated from Fig.5 where we compare [Fe/H] distributions in the three simulations.

3.1 Assembly histories

In order to understand if the stars in each component were formed *in situ* (i.e. in the main progenitor of the final galaxy) or in smaller objects which were subsequently accreted, we follow each star from its time of formation to $z = 0$. This allows us to estimate the fraction of stellar mass in each component which formed *in situ*. We consider all self-bound bound clumps of more than 20 simulation particles to be separate objects, so that any star which formed in a clump other than the main progenitor is considered to have been accreted.

Cumulative *in situ* and accreted fractions are shown in Fig. 6 as a function of the redshift at which the stars formed. The four panels give results for our four stellar components, and within each panel solid lines give *in situ* fractions while dashed lines give accreted fractions. Different colours refer to the different Aquarius galaxies as noted in the caption. Most of the stellar mass in the central spheroids was formed *in situ* varying from ~ 60 to ~ 95 per cent. Only in Aq-F-5, which underwent a major merger at $z \sim 0.6$, are the *in situ* and accreted fractions comparable. In contrast, in the outer stellar haloes the majority of the stars are accreted in all eight galaxies. (Remember that we have excluded stars which remain part of a bound satellite at $z = 0$ when compiling these statistics.) The inner haloes show an intermediate behaviour with both fractions ranging between 25 and 75 per cent. About 75 per cent of the inner halo of Aq-F-5 is accreted, most of it as part of the second object in the major merger. The $z = 0$ discs are heavily dominated by *in situ* stars, with a maximum accreted contribution of ~ 15 per cent. Note however, that the largest accreted fractions are for Aq-E-5, where Figs 1 and 2 show there to be no clear separation between disc and inner halo, and Aq-H-5, where the disc component is very weak.

To correlate assembly histories with chemical abundances, we compare the fraction of stars formed *in situ* ($F_{\rm prog}$) in each stellar component to the median abundance of the stars at $z = 0$. In Fig. 7 we show medians of [Fe/H] as a function of $F_{\rm prog}$ (upper panel). As can be seen, stellar components become more metal-rich as one moves inward; the central spheroid is always much more chemically enriched than the corresponding outer halo. The trends are encouragingly consistent with Milky Way data. The median [Fe/H] of central spheroids appears independent of *in situ* fraction, whereas in the outer halo is there a clear trend for higher [Fe/H] to correspond to smaller *in situ* fraction.

In the lower panel of Fig. 7 we plot median [O/Fe] against $\rm F_{prog}$. The weak α-enhancement of disc stars is a

Table 5. Chemical properties of the inner diffuse stellar haloes. The first column shows the encoding name of the simulations. $F_{\rm prog}$ and $F_{\rm prom}$ are the fractions of stars formed in the progenitor systems and of stars which have been part of a galactic wind. σ and Age are the mean velocity dispersion (in km s^{-1}) and mean age (in Gyr), respectively. [Fe/H] and [O/Fe] are median abundances. Standard deviations are included within parentheses. The labels "prog" and "sat" denote the values corresponding to stars formed *in situ* and to stars acquired from satellites.

Halo	$F_{\rm prog}$	$F_{\rm prom}$	[Fe/H]$^{\rm prog}$	[Fe/H]$^{\rm sat}$	[O/Fe]$^{\rm prog}$	[O/Fe]$^{\rm sat}$	Age$^{\rm prog}$	Age$^{\rm sat}$
Aq-A-5	0.75	0.15	-1.17(0.52)	-1.45(1.07)	0.060(0.145)	0.351(0.054)	10.40(4-05)	12.60(0.15)
Aq-B-5	0.32	0.27	-1.37(0.85)	-1.24(0.79)	0.031(0.150)	0.113(0.223)	10.45(1.94)	10.12(2.33)
Aq-C-5	0.56	0.26	-1.05(0.81)	-1.20(0.8)	0.002(0.141)	0.311(0.008)	11.50(0.92)	12.37(0.40)
Aq-D-5	0.57	0.27	-1.09(0.54)	-1.03(0.75)	-0.079(0.135)	0.152(0.146)	9.96(2.67)	11.47(0.53)
Aq-E-5	0.47	0.43	-0.84(0.51)	-0.86(0.63)	-0.049(0.139)	0.028(0.154)	10.29(4.12)	11.16(0.76)
Aq-F-5	0.25	0.39	-1.05(0.59)	-0.87(0.68)	-0.002(0.131)	-0.024(0.184)	9.44(5.59)	9.76(3.89)
Aq-G-5	0.59	0.35	-1.03(0.58)	-1.02(0.93)	0.019(0.126)	0.043(0.177)	11.05(1.89)	10.47(2.13)
Aq-H-5	0.54	0.46	-0.79(0.49)	-0.87(0.67)	-0.056(0.175)	0.148(0.420)	10.88(2.10)	11.82(0.88)

Table 6. Chemical properties of the outer diffuse stellar haloes. The first column shows the encoding name of the simulations. $F_{\rm prog}$ and $F_{\rm prom}$ are the fractions of stars formed in the progenitor systems and of stars which have been part of a galactic wind. σ and Age are the mean velocity dispersion (in km s^{-1}) and age (Gyr)of the stars. [Fe/H] and [O/Fe] are median abundances. Standard deviations are included within parentheses. The labels "prog" and "sat" denote the values corresponding to stars formed *in situ* and to stars acquired from satellites.

Halo	$F_{\rm prog}$	$F_{\rm prom}$	[Fe/H]$^{\rm prog}$	[Fe/H]$^{\rm sat}$	[O/Fe]$^{\rm prog}$	[O/Fe]$^{\rm sat}$	Age$^{\rm prog}$	Age$^{\rm sat}$
Aq-A-5	0.35	0.20	-2.04(1.25)	-1.44(1.31)	0.018(0.168)	0.145(0.203)	10.79(3.93)	11.08(2.14)
Aq-B-5	0.13	0.12	-1.59(1.39)	-1.70(1.12)	0.019(0.154)	0.119(0.307)	10.14(2.43)	9.28(2.58)
Aq-C-5	0.19	0.21	-2.04(1.46)	-1.31(1.14)	0.054(0.149)	0.089(0.205)	11.54(0.92)	11.29(1.11)
Aq-D-5	0.19	0.24	-1.76(1.24)	-1.36(1.07)	0.018(0.160)	0.100(0.249)	10.59(2.47)	11.08(1.22)
Aq-E-5	0.25	0.20	-1.66(1.17)	1.39(1.16)	0.019(0.155)	0.079(0.242)	10.82(1.52)	11.32(1.67)
Aq-F-5	0.03	0.23	-2.11(1.65)	-1.32(1.09)	0.019(0.160)	0.019 (0.302)	11.14(6.99)	9.64(3.41)
Aq-G-5	0.25	0.05	-1.78(1.44)	-1.85(1.22)	0.018(0.161)	0.089(0.320)	10.55(6.45)	10.54(4.07)
Aq-H-5	0.15	0.29	-1.73(1.64)	-1.21(1.02)	0.022(0.136)	0.075(0.222)	11.80(2.36)	11.21(1.21)

consequence of the bursty and extended star formation activity which gives rise to this component, allowing new stellar populations to form from material enriched by SNIa. Our SN feedback model allows us to track gas particles which have been promoted from the cold to the hot phase, thus becoming part of a galactic wind. We have checked how much of each disc formed from gas that was ever part of a wind, finding this to vary between ~ 10 and ~ 30 per cent. Hence, the great majority of disc stars formed from material that was acquired directly by infall and was enriched *in situ* without cycling through a galactic fountain.

In central spheroids the level of α-enrichment increases with *in situ* fraction as indicated by the median abundances in Fig. 7 (lower panel). This is also consistent with the age distribution of these stars which, in general, are old, forming in strong starbursts which are too short for SNIa enrichment to be important (Fig. 3). We find that more than 40 per cent of the stars in our central spheroids formed from gas that had been promoted at least once, showing that these dense and strongly bound regions are able to retain much of their SN ejecta. Since these regions are α-enhanced, the cooling and re-accretion of the promoted gas particles had to occur in less than ≈ 1 Gyr.

The outer and inner stellar haloes are more α-enhanced than the central spheroids. For these components, the fraction of stars formed from gas that had participated in a wind varies from 5 to 50 per cent, with the largest fractions of such stars in the inner haloes. We found that these 'recycled-material' stars are primarily accreted rather than *in situ* objects, so were typically formed in satellite galaxies which were later disrupted. This is a consequence of our SN feedback model which results in larger promotion rates (relative to the star formation rate) in systems with shallower potential wells: smaller haloes experience more significant winds (Scannapieco et al. 2008; Sawala et al. 2010; De Rossi et al. 2010; Sawala et al. 2011).

So far we have analysed the abundance distribution of our stellar components without regard to where the stars formed. However, there are different levels of α-enrichment in the three spheroidal components, even though all are dominated by old populations with quite similar star formation histories. This suggests that the assembly history of each component plays an important role. Hereafter, we focus on this point.

Properties of the *in situ* and accreted subpopulations of each component in each Aquarius galaxy are listed in Tables 3 to 6. Each table refers to a different component and gives for each galaxy the stellar fractions formed *in situ* and from previously promoted gas, as well as the median [Fe/H] and [O/Fe] and the mean stellar age separated into *in situ* and accreted components.

The *in situ* stars in discs have younger and more diverse ages than those of any other (sub)population, as can be seen from the penultimate column in Table 3. In particular, the few disc stars acquired from disrupted satellites are not only older but formed, on average, over shorter time intervals. As

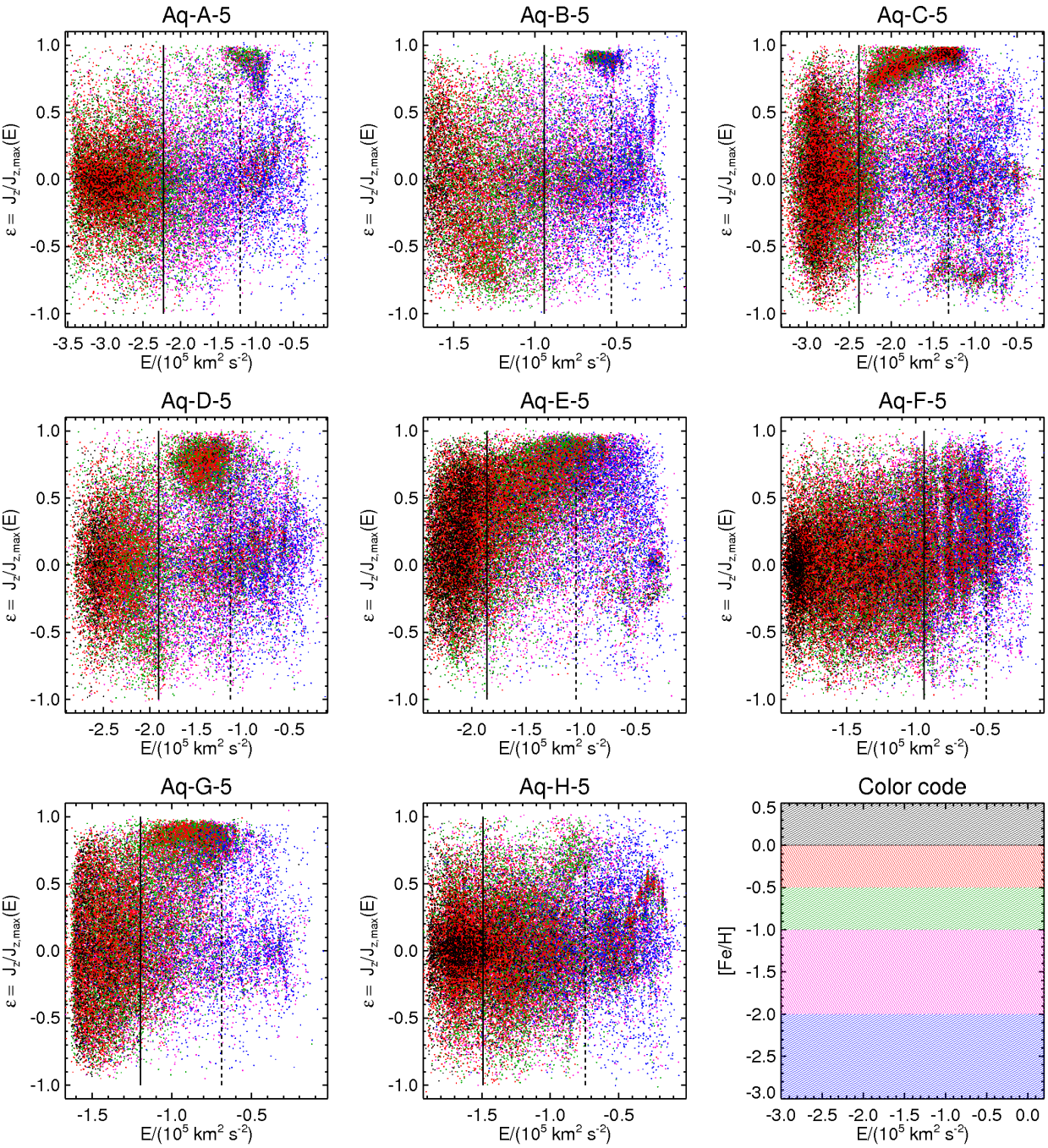

Figure 1. Distribution of $\epsilon = J_z/J_{z,\max}(E)$ as a function of energy E for our eight Aquarius haloes. The last panel shows the color code used to represent the [Fe/H] abundances of star particles. Energies have been zero-pointed at the value for a circular orbit at the virial radius. The energies which separate our three spheroidal components are indicated for galaxy system in the relevant panel. For the sake of clarity, only 10% of the particles are displayed.

a consequence, these stars tend to have lower metallicity and to be more α-enhanced than the *in situ* disc population. *In situ* disc populations also tend to have lower velocity dispersions than accreted disc populations (see columns 4 and 5 of Table 3). This suggests that accreted stars should contribute primarily to the metal-poor end of a thick disc component (Abadi et al. 2003; Wyse 2010).

Our central spheroids are populated primarily by old stars which formed *in situ* over a relatively short time interval ($\sim$ 1.5 to 4 Gyr; see Table 4). The exceptions are Aq-E-5 and Aq-F-5, which have been significantly rejuvenated by younger stars, as indicated by their larger age dispersions. Generally, accreted stars in the central spheroids tend to be older, to have formed over very short intervals, to have lower metallicities and to be more α-enhanced than those formed *in situ*.

Our inner stellar haloes are formed by a mixture of *in situ* and accreted stars (Table 5). In general, the latter have

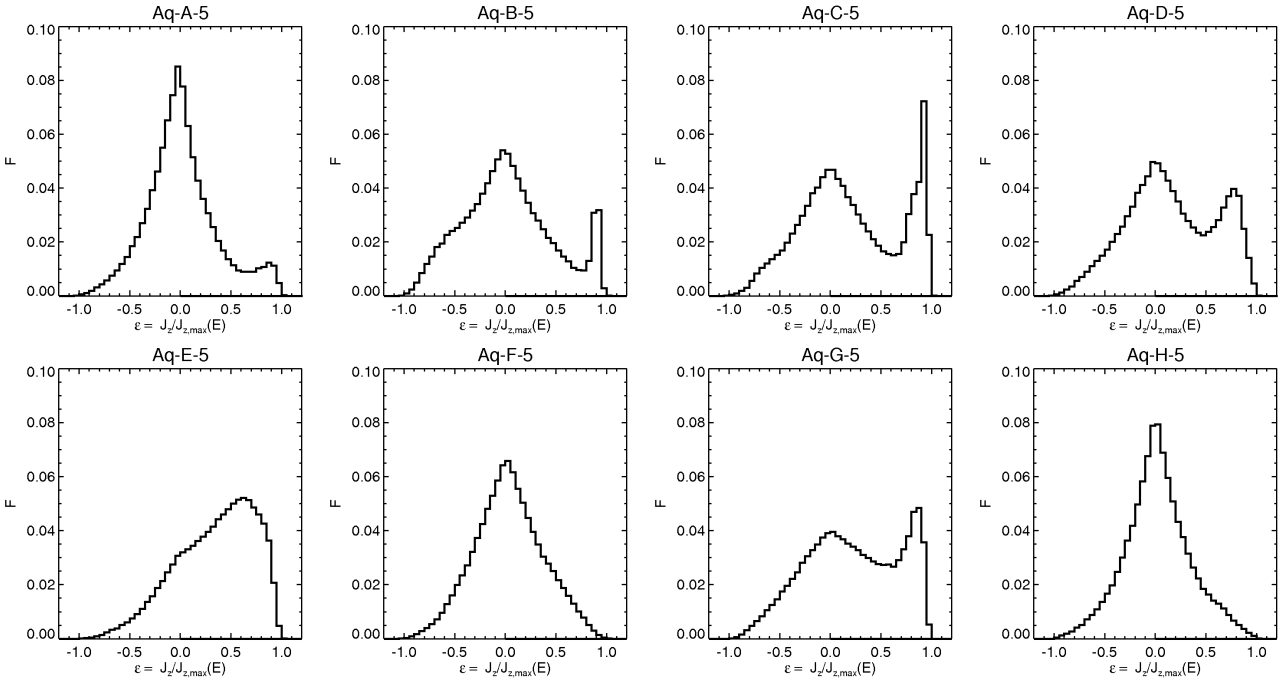

Figure 2. Histograms of stellar mass as a function of $\epsilon = J_z/J_{z,\max}(E)$ for our Aquarius haloes within twice $r_{\rm gal}$ at $z = 0$. Stars in satellites have been excluded.

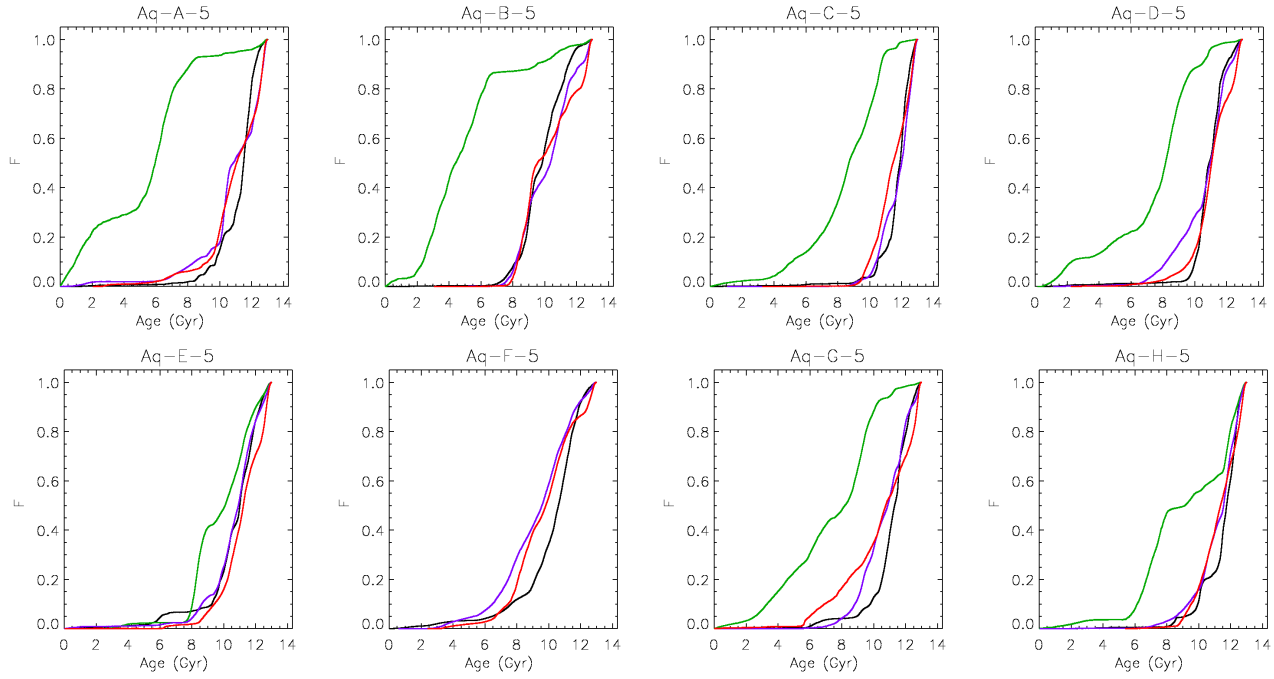

Figure 3. Cumulative stellar mass as a function of age for stars in the disc (green), the central spheroid (black), the inner halo (violet) and the outer halo (red) for all simulated galaxies.

similar metallicities but higher α-enhancements. They also tend to be older and to have formed over a shorter period of time. Similar trends hold for stars in the outer haloes (Table 6), although in this case accreted stars tend to be more metal-rich as well as to have higher α-enhancements than the *in situ* population and there is no clear age separation between the two populations. Apparently, at least a small fraction of outer halo stars formed *in situ* from SNIa enriched material. These may also have formed at lower redshift, giving rise to the large age dispersions listed for several galaxies in Table 6. Recall that stars formed *in situ* account for less than 20 per cent of the stellar mass in the outer

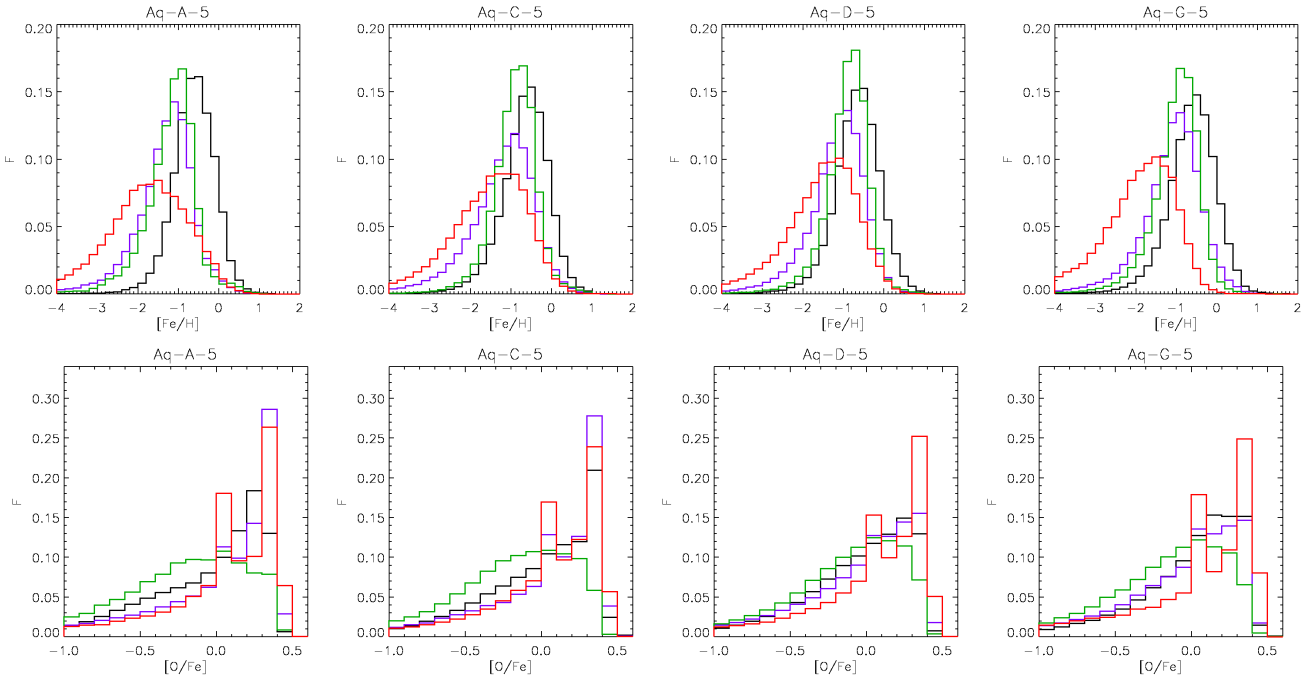

Figure 4. Distributions of [Fe/H] (upper raw) and [O/Fe] (lower raw) for stars in the discs (green), central spheroids (black),inner stellar haloes (violet) and outer stellar haloes (red) of four Aquarius galaxies.

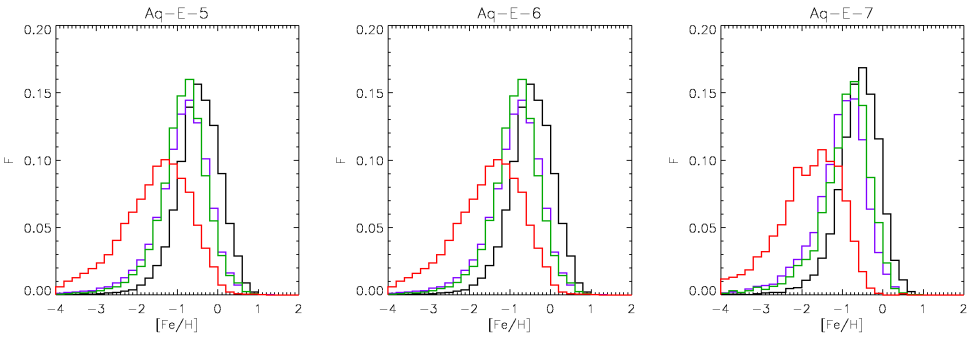

Figure 5. Distributions of [Fe/H] for stars in the discs (green), central spheroids (black),inner stellar haloes (violet) and outer stellar haloes (red) of Aq-E sampled at three different levels of resolution, declining from Aq-E-5 to Aq-E-7.

haloes and that all bound satellites have been removed and are considered as separate objects. Hence, we are here focussing on the "smooth" component of stellar haloes. Our stellar haloes have a dual formation process since the ratio of accreted to *in situ* stars typically increases from 1 to 5 between the inner and outer haloes (see also Zolotov et al. (2009)). We will explore this issue in more detail in the next section.

Old metal-rich stars can be viewed as chemical fossils (Bland-Hawthorn & Freeman 2003). We have measured the fraction of stars both older than 11 Gyr and with [Fe/H]>0 in each component of each of our simulated galaxies. As expected the largest fractions are found in the central spheroids, ranging from eight down to one per cent. The other components have very few stars with these characteristics (fractions always below 1%). This is consistent with the fact that only in deep potential wells is it possible to reach high levels of enrichment in such a short period of time. Although we find no correlation with $F_{\rm prog}$, we did detect a trend with the strength of the first starbursts: those central spheroids with a large fraction of old metal-rich stars have more than 40 per cent of their total stellar mass already formed at $z > 3$ (i.e. older than 11 Gyr). Conversely, the other central spheroids were able to form less than 25 per cent of their final stellar mass by this time. The lowest fraction of old metal-rich stars is found in Aq-B-5 which made only 15 per cent of its final stellar bulge by $z \sim 3.5$. Hence, the fraction of old and metal-rich stars in the central spheroids is linked to how fast star formation proceeded in the first massive structures and so is of interest for constraining galaxy formation models, as claimed in previous work (e.g. Wyse 2010, and references therein).

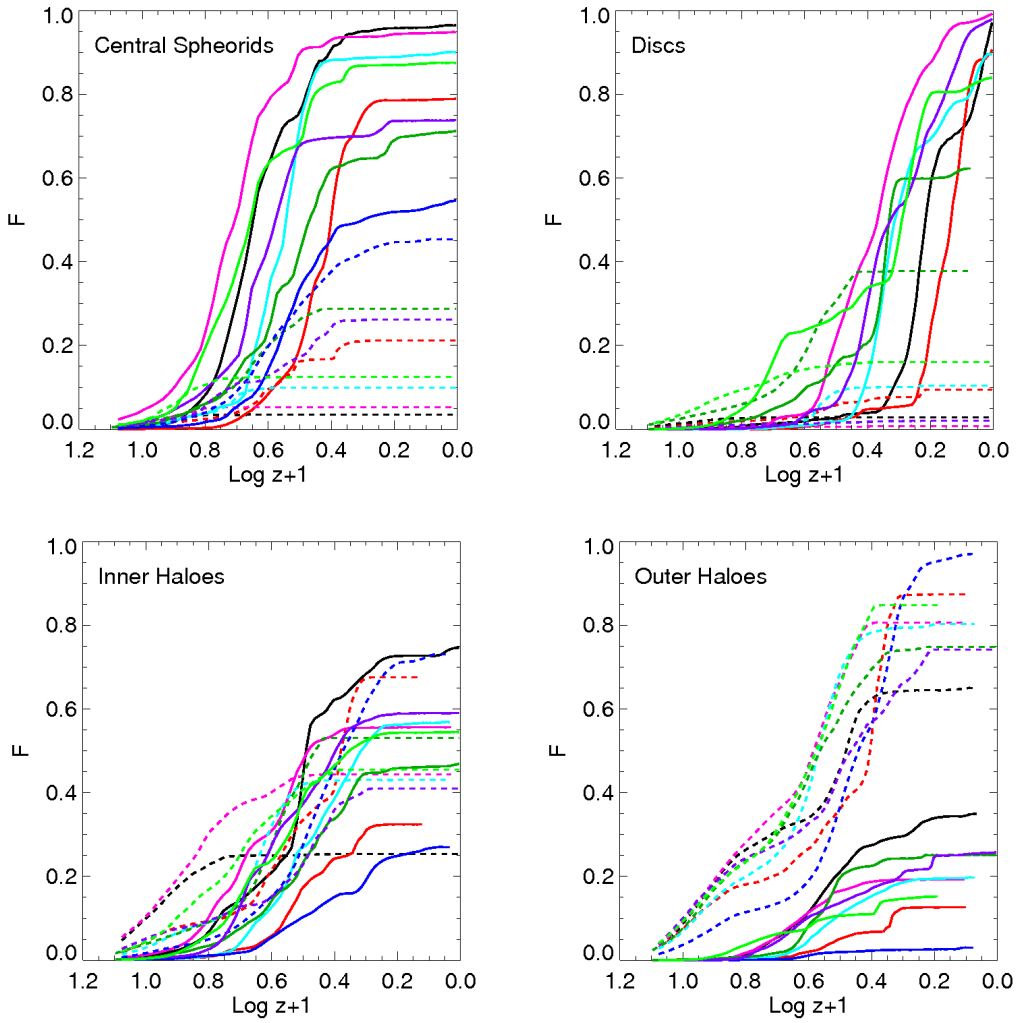

Figure 6. Accreted (dashed) and *in situ* (solid) fractions as a function of formation redshift for stars in each of our four components and for all eight of the Aquarius galaxies. Each of the panels corresponds to a different component as labelled, while the colours of the curves identify the individual galaxies. The key is: Aq-A-5 (black), Aq-B-5 (red), Aq-C-5 (magenta), Aq-D-5 (cyan), Aq-E-5 (green), Aq-F-5 (blue), Aq-G-5 (violet) and Aq-H-5 (light green).

4 THE INFLUENCE OF THE MASSES OF DISRUPTED SATELLITES ON THE ABUNDANCE PATTERNS OF ACCRETED COMPONENTS

The abundance patterns of the various components of our simulated galaxies depend on the fraction of their stars which was accreted. However, the dispersions in these relations are large, suggesting that other factors are also important. In particular, the masses of the disrupted satellites vary from halo to halo (e.g. Cooper et al. 2010) and these differences could be reflected in the chemical patterns. In order to investigate this issue, we estimate the percentage ($F_{\rm massive}$) of the total stellar mass in a given dynamical component formed in satellites with stellar masses larger than a certain value. As can be seen in Fig. 8, the stellar mass of contributing satellites varies widely. The variation is particularly marked for the inner and outer stellar haloes which were assembled primarily from satellite debris. As a reference value for $F_{\rm massive}$ we take that measured for stellar mass $5\times10^9 M_\odot h^{-1}$, similar to the stellar masses of the surviving satellites at $z=0$ in the Aquarius simulations[3].

In Fig. 9, we show the mass fraction of stars formed in satellites more massive than $5\times10^9 M_\odot h^{-1}$ ($F_{\rm massive}$) as a function of $F_{\rm prog}$. There is a clear anti-correlation which simply reflects the fact that the larger the mass fraction formed in satellites, the larger the chance that massive objects have contributed. In the discs and central spheroids, which formed primarily *in situ*, the accreted stars come mainly from small satellites (i.e. at most ~ 20 per cent from massive ones). The central spheroids of Aq-E-5 and Aq-F-5 show the largest accreted fractions and a substantial fraction of their stars come from massive satellites, $\sim 0.30-0.40$ per

[3] Note that we do not use the ratio between the mass of the progenitor and that of the satellite because metallicities are related to the total stellar mass which could have enriched the system and to its potential well which affects the overall star formation efficiency and the impact of outflows.

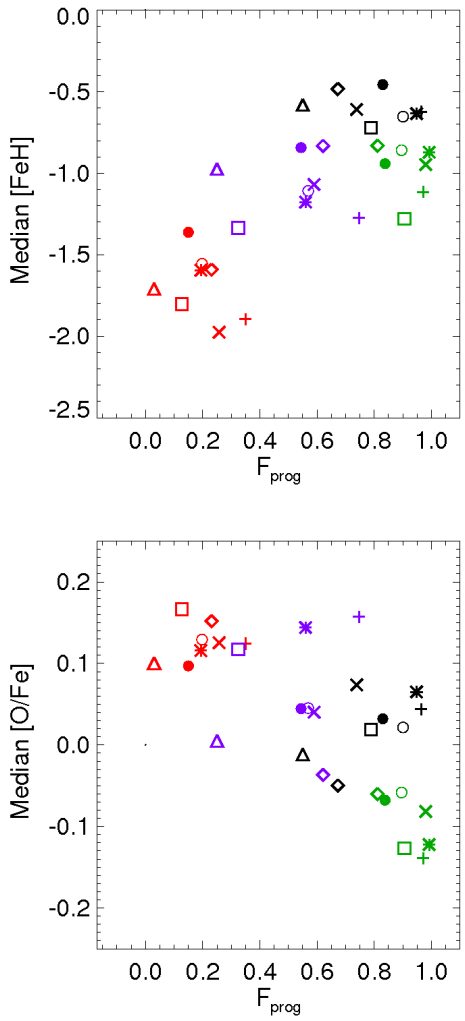

Figure 7. Medians of [Fe/H] and [O/Fe] as a function of $F_{\rm prog}$ for central spheroids (black), discs (green), inner haloes (violet) and outer halos (red). Symbols differentiate the eight galaxies: Aq-A-5 (cross), Aq-B-5 (square), Aq-C-5 (asterisk), Aq-D-5 (open circle), Aq-E-5 (diamond), Aq-F-5 (triangle), Aq-G-5 (ex) and Aq-H-5 (filled circle).

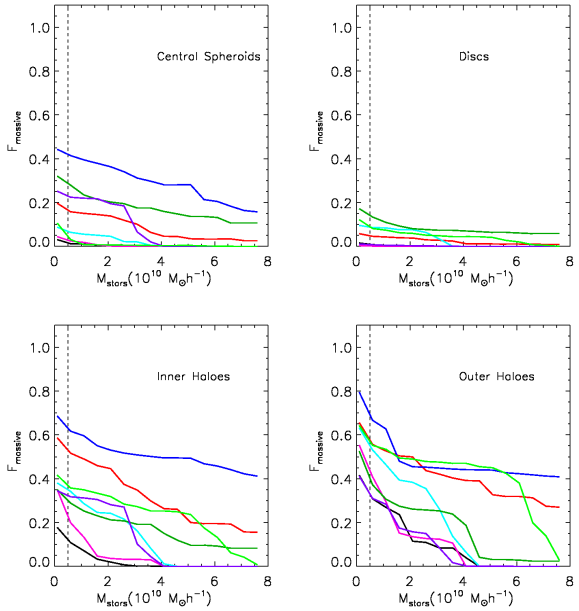

Figure 8. Fraction by mass of each stellar component acquired from satellites more massive than a given stellar mass as a function of this stellar mass. The dashed lines denote the reference stellar mass, $5 \times 10^9 M_{\odot} h^{-1}$ See Fig.6 for the colour code.

cent, consistent with the fact that they alsos show the lowest median [O/Fe] (Fig.7). The outer and the inner haloes have the largest contributions from stars accreted from massive satellites while the lowest such contributions are found in discs. As we show in Fig. 8, the mass functions of the contributing satellites vary significantly from galaxy to galaxy, leaving their imprints on the chemical abundances.

In Fig. 10, we show the [Fe/H] and [O/Fe] medians as a function of $F_{\rm massive}$. The stellar populations of the inner and outer haloes tend to be more metal-rich when larger fractions of their stars are accreted from massive satellites (see Fig. 10, upper panel). In this case, the correlation is clearer than that with the fraction of *in situ* stars. The inner haloes of Aq-B-5 and Aq-F-5 show similar levels of enrichment to their outer haloes. From Fig. 8 we see that the outer and inner haloes of these particular galaxies have similarly important contributions from stars formed in massive systems, while for the other galaxies, the contribution of stars acquired from massive satellites decreases significantly as one moves from the inner to the outer stellar halo. Thus, the stellar masses of the satellites where accreted stars were formed is an important factor in determining their mean level of enrichment: more metal-rich halo stars tend to come from more massive satellites.

As shown in Fig. 10 (lower panel), α-enhancement tends to increase with a decreasing contribution from massive satellites for all three spheroidal components. The lowest median [O/Fe] values are found in central spheroids. Inner haloes extend over a larger range of both [O/Fe] and $F_{\rm massive}$, while outer stellar haloes show the highest α-enhancements, reflecting the fact that they are dominated by old stars formed during short starbursts.

A dual origin for halo stars is suggested by observations of the Milky Way which show the inner halo to have a stellar metallicity distribution peaking at [Fe/H]≈ -1.6 while the outer halo is dominated by less enriched stars with peak [Fe/H]≈ -2.2 (Carollo et al. 2007). There are also new observations suggesting differences in kinematics and α-enrichment for stars in the Milky Way stellar halo which might indicate the presence of two distinct stellar populations (e.g. Nissen & Schuster 2010; Beers et al. 2011). We now explore if the relative abundances of the inner and outer stellar field haloes of the Aquarius systems are comparable to these observed values and if a radial trend is a common characteristic of all our simulated systems. We stress the fact that in this section, we are analysing the diffuse stellar population in each component. Surviving satellites are explored in the last section of this paper.

We have estimated the differences in median [Fe/H] between the inner and outer stellar haloes of each of our eight simulated galaxies and looked for relations to the fraction of *in situ* stars. In all systems, the outer halo is less chemically

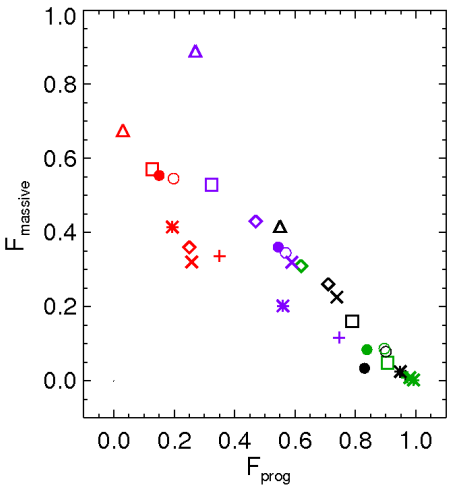

Figure 9. Fraction by mass of each stellar components accreted from satellites with stellar masses larger than $5 \times 10^9 M_\odot h^{-1}$ ($F_{\rm massive}$) as a function of $F_{\rm prog}$. See Fig.7 for the symbol code.

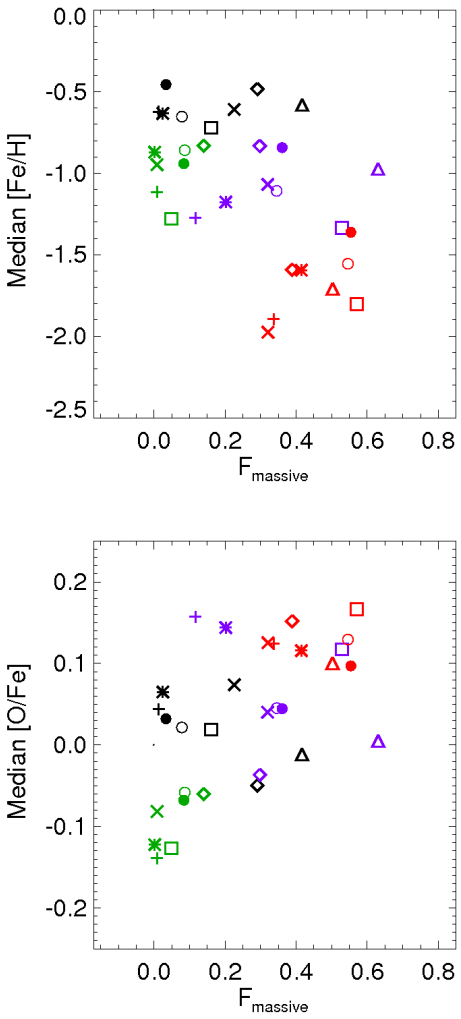

Figure 10. Median [Fe/H] and median [O/Fe] as a function of $F_{\rm massive}$, the mass fraction of stars accreted from satellites with virial masses larger than $5 \times 10^9 M_\odot h^{-1}$. See Fig.7 for symbol code.

enriched than the inner one, with differences varying from ~ -0.6 dex to ~ -1.0 dex (Fig. 11). The values quoted by Carollo et al. (2007) for the Milky Way imply a difference of ~ -0.6 dex, consistent with the range in the simulations where these gradients reflect the gradients in assembly history. Zolotov et al. (2009) and Zolotov et al. (2010) reached similar conclusions, but used a different approach, so caution is needed in any detailed comparison with our results. The dispersion in chemical gradients reflects a variety of factors, including the accreted mass fraction, the mass function of disrupted satellites, the ages of their stars, the mixing effiency, and the strength of outflows. For example, Aq-G-5 has the largest chemical differences between the inner and outer haloes due to a larger contribution of debris from massive satellites to the inner halo than to the outer one. α-enhancements depend principally on the star formation timescales and the level of chemical mixing both in disrupted satellites and in the main progenitor systems. The inner haloes of our Aquarius galaxies are typically ~ 0.8 dex less α-enhanced than their outer haloes, but in Aq-A-5 and Aq-C-5 the inner haloes are slightly more α-enriched than their outer components for given $\Delta F_{\rm prog}$. Fig. 8 shows that these two inner haloes obtained their accreted stars from much smaller satellites than the corresponding outer haloes, contrasting with the other Aquarius systems.

A similar comparison can be done for the central spheroids and the inner haloes. In this case we found metallicity differences ranging from 0.9 to 0.4 dex with central spheroids always more enriched than the inner haloes. Based on observations reported in the literature (e.g Wyse 2010), we estimate a corresponding difference of ~ 0.35 in the Milky Way, in reasonable agreement with our results even though none of our simulated systems has a morphology resembling that of the Milky-Way. These trends are shown in Fig.11. Larger differences in metallicity, are again associated with larger differences in formation history between the two components. The central spheroids are also systematically less α-enriched than the inner haloes, and again this trend is more important for larger differences in the way the components were assembled.

5 SURVIVING SATELLITES

The chemical abundances of Milky Way satellites and nearby dwarf galaxies have been a subject of much research. Observations suggest significant differences between the abundance patterns of stars in the Galactic halo and those in dwarf galaxies: stars in dwarfs tend to have lower [α/Fe] than similar metallicity stars in the Galactic halo (e.g. Tolstoy et al. 2003) even at low [Fe/H] levels. Thus it appears that the Galactic halo could not have been built from systems similar to the current satellites. In this Section, we compare these two populations in our simulated systems. For this analysis, we have only considered satellites represented by more than 2000 total particles. Two of our galaxies (Aq-E-5 and Aq-H-5) are excluded from this analysis, since they have no satellites satisfying this numerical requirement.

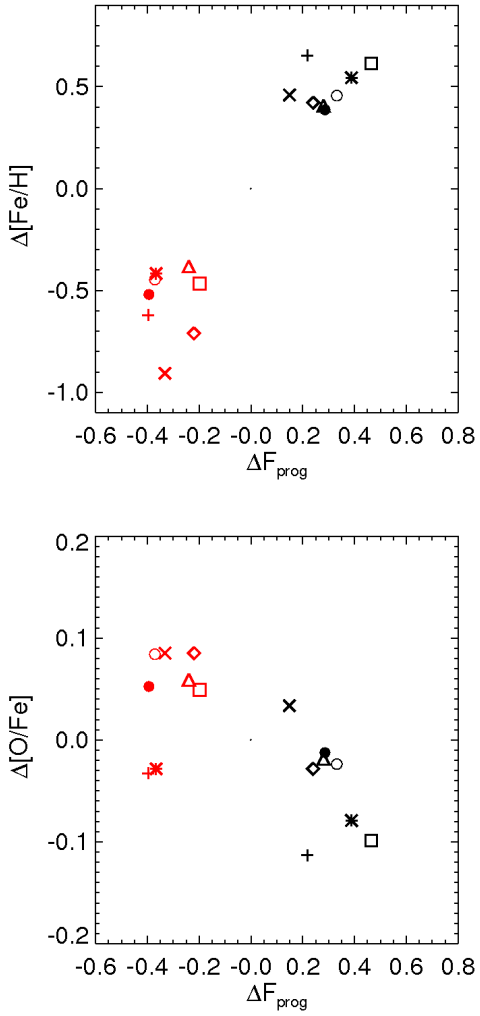

Figure 11. [Fe/H] and [O/Fe] abundances of central spheroids relative to inner stellar haloes (black symbols) and of outer stellar haloes relative to inner haloes (red symbols) haloes as a function of the differences between the fractions of stellar mass formed *in situ* ($\Delta F_{\rm prog}$). See Fig. 7 for the symbol code.

In Fig. 12, we show cumulative stellar mass as a function of stellar age for each satellite of the remaining six galaxies. Clearly, star formation histories differ considerably, with most showing several starburst episodes. For comparison, we have included the star formation histories of the outer haloes of the corresponding systems. Most surviving satellites have experienced several starbursts and are dominated by younger stellar populations than the corresponding outer haloes. Few satellites have significant old stellar populations and only one halo, Aq-B-5, has satellites dominated by older stars than those in the corresponding outer halo. This figure shows the variety in the star formation histories of satellites inhabiting similar haloes, illustrating the difficulty of comparing the Milky Way to any specific simulation. For this reason, we compare the chemical properties of accreted stars in our four stellar components to those of stars in the surviving satellites on a statistical basis.

Fig. 13 shows the distributions of median [O/Fe] and median [Fe/H] for stars in surviving satellites (solid lines) and for accreted stars in the outer haloes (dotted lines). Accreted stars tend to be α-enhanced, reflecting the fact that they formed quickly and in short bursts, so that SNII enriched them but SNIa exploded too late to affect their abundances. In contrast, surviving satellites contain significantly more weakly α-enhanced stars at all metallicities. This is a consequence of their extended star formation histories (Fig. 12). As shown in previous papers, our feedback model successfully drives mass-loaded galactic winds out of star-forming galaxies with a wide range of masses, and with a specific mass-loss rate which depends on the potential well depth of the systems. These winds regulate star formation activity and determine the fraction of available baryons which are turned into stars (Scannapieco et al. 2008, 2009, 2010; Sawala et al. 2010; De Rossi et al. 2010; Sawala et al. 2011). As a result, the chemical properties and ages of the stars in surviving satellites are statistically different in our simulations from those of stars acquired by satellite disruption.

An interesting point of comparison between our current model and observation concerns the percentage of very metal-poor stars ([Fe/H] < -3) in the surviving satellites. In our simulations this varies from 0.5 to 20 per cent (with an average of ~ 10 per cent), depending on details of individual star formation histories. These stars are α-enhanced and old. The apparent lack of such low-metallicity stars in real systems has been suggested as a possible problem for hierarchical galaxy formation models in the past (e.g. Shetrone et al. 2001; Helmi et al. 2006). However, more recent studies have discovered extremely metal-poor stars in dwarf galaxies (Kirby et al. 2008, 2009; Norris et al. 2008, 2010). These new observations, together with improved metallicity indicators (Starkenburg et al. 2010), are causing a revision of ideas about the low metallicity tail of the stellar populations, which are clearly more extensive than previously thought. These tails are of great interest for investigations of the possible impact of other processes such as pre-enrichment by Population III stars which might have led to a floor for Population II metallicities, leading to a deficit of extremely metal-poor stars in dwarfs. Improved observational surveys of low metallicity stars in nearby satellites are thus very much relevant for constraining galaxy formation models.

Our results are encouraging in that they show differences between the chemical properties of accreted halo stars and those of stars in surviving satellites which are quite similar to the trends observed in the Milky Way. Higher resolution simulations are clearly needed to confirm these findings, but they already suggest that these trends are not only compatible with the standard model of hierarchical formation in a ΛCDM cosmology, but may, indeed, provide direct evidence for the assembly paths it predicts.

6 CONCLUSIONS

In this paper we study the chemical patterns of the stellar populations in eight Milky-Way mass-sized galaxies simulated within the ΛCDM scenario. Our version of GADGET-3 includes the modelization of SN feedback describing the release of energy and chemical elements in the interstellar medium so that the chemical enrichment of baryons can

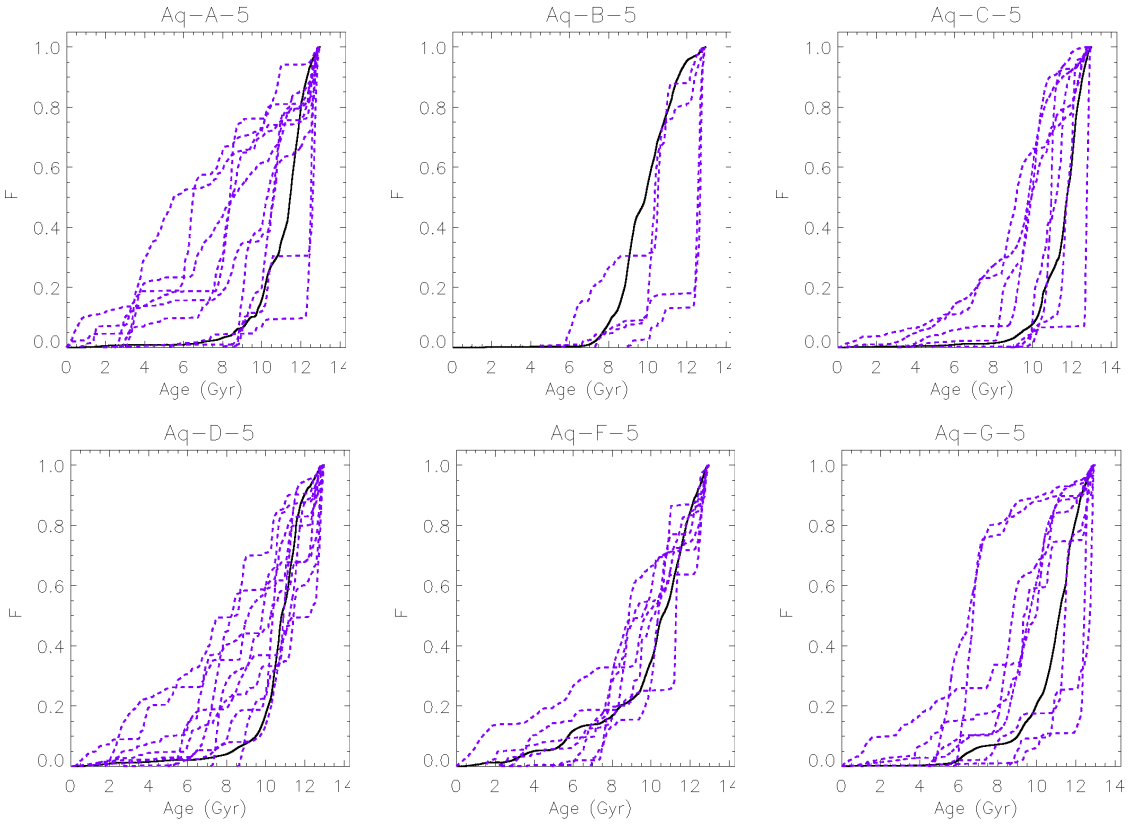

Figure 12. Cumulative stellar mass as a function of age for surviving satellites (violet dashed lines) and for the outer stellar haloes (black solid lines) of six of our Aquarius galaxies. Aq-E-5 and Aq-H-5 have only very low-mass satellites and have not been included in this plot.

be followed consistently as galaxies are assembled. This is the largest sample of high resolution Milky-Way mass-sized galaxies so far run with a physical motivated SN model fact that provides us with the unique possibility to distinguish those chemical properties which are common to all galaxies from those that are determined by the particular history of assembly of each galaxy.

Our results can be summarized as follows

• Discs: The surviving discs show very similar chemical properties. They are more chemically enriched than the stellar halo but slightly less enriched than the central spheroids. The stars in discs show the lowest levels of α-enhancement. This is consistent with being formed from SNIa pre-enriched material. These stars formed mainly *in situ*. Most of the stars in the discs formed from material which has never been part of a galactic wind. In general, the discs formed inside-out as shown by Scannapieco et al. (2009, 2011), and during this process different starbursts enriched continuously the gas. We identified that up to 15 per cent of the stars in the discs formed in satellite systems confirming previous results (Abadi et al. 2003). These stars tend to older and formed in shorter starbursts in comparison to the dominating stellar population formed *in situ*. Accreted stars have systematically higher α-enhancement and are more supported by velocity dispersion. These stars could contribute to a thick disc component. Most of the accreted stars come from satellites smaller than $5 \times 10^9 \mathrm{M}_\odot h^{-1}$ total stellar mass.

• Central spheroids: They are formed mainly by old stars, born in starbursts with different duration ranging from 2 to 4 Gyrs approximately. The stellar populations in central spheroids have been formed *in situ* with contributions of less than ~ 20 per cent of stars formed in satellites. Two systems out of eight (Aq-E-5 and Aq-F-5), show larger contributions of accreted stars. These central spheroids have been also recently rejuvenated by news stars formed mainly *in situ* by the infall of enriched gas(mean stellar age of the new population 4-5 Gyrs). This can be confirmed by the lower α-enhancement showed by these two central spheroids with respect to the rest of the systems. Very old and metal-rich stars are principally located in the central spheroids and their frequency can be correlated with rate of star formation in the earliest epoch of formation.

• The inner and outer field haloes: As one moves outward the contribution from disrupted stars to the field stellar haloes increases dramatically. The inner haloes have contribution from both kind of stars, but the outer haloes have been mainly formed by accreted stars. The mean metallicity shows a large dispersion which correlates with the fraction of stars acquired from massive satellites (i.e. larger than $5 \times 10^9 \mathrm{M}_\odot h^{-1}$) so that the larger this fraction, the larger the mean level of enrichment of the halo. This is valid for both the inner and the outer haloes.

We find that in all simulated stellar haloes the stars in the outer region are systematically less enriched. The differences in the chemical properties between the inner and the outer

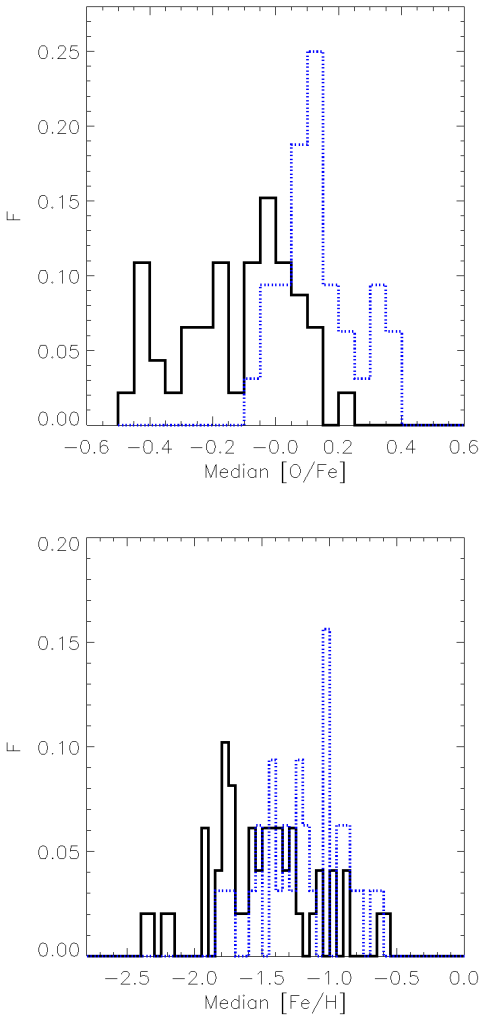

Figure 13. Distributions of median [O/Fe] (upper panel) and of median [Fe/H] (lower panel) for the accreted component of outer haloes (dotted lines) and for stars in surviving satellites (solid lines).

field haloes are not only the consequence of the different relative contributions of *in situ* and accreted stars (Zolotov et al. 2009) but also reflect the mass function of the satellites which contributed with stars to form them.

The level of α-enhancement is higher in outer field stellar haloes reflecting the fact that they have been mainly assembled from old stars formed in smaller structures, in single short-duration starbursts. Only stars accreted from very massive systems tend to be, on average, less α-enriched at a given metallicity than the global population of the halo (Zolotov et al. 2010). The masses of the specific satellites where the accreted stars were formed are reflected in the chemical properties of the inner and outer haloes, imprinting features which distinguish one system from another.

• Surviving satellites: Each simulated Milky-Way mass galaxy has a system of surviving satellites with particular characteristics. The surviving satellites show a variety of star formation histories but in general, they formed stars in a series of starburst episodes which extended even to the present time. As a consequence, their chemical patterns differ from those of the stars that contributed to the formation of the stellar components of the main galaxies. On average, stars in surviving satellites are younger, low metallicity and low α-enriched.

Although there are many open questions and issues to be solved regarding galaxy formation, particularly those that could be related to the formation and surviving of disc galaxies, it is encouraging that the global chemical trends observed in nearby galaxies can be obtained in ΛCDM scenarios. Our work shows the importance of studying chemical evolution to understand galaxy formation and the relevance of doing so within a cosmological context.

ACKNOWLEDGEMENTS

We thank the referee, Brad Gibson, for his useful comments which helped to improve this paper. PBT thanks Manuela Zocalli, Patricia Sanchez-Blazquez and Tim Beers for their suggestions and comments and the ISIMA at University of Santa Cruz for the stimulating environment that helped to put this paper together. This work was partially funded by PROALAR 07 (DAAD-Secyt collaboration), PICT 32343 (2005) and PICT Max Planck 245 (2006) of the Ministry of Science and Technology (Argentina).

REFERENCES

Abadi M. G., Navarro J. F., Steinmetz M., Eke V. R., 2003, ApJ, 591, 499
Agertz O., Teyssier R., Moore B., 2009, MNRAS, 397, L64
Agertz O., Teyssier R., Moore B., 2011, MNRAS, 410, 1391
Barnes J. E., Hernquist L., 1996, ApJ, 471, 115
Beers T. C., Carollo D., Ivezic Z., An D., Chiba M., Norris J. E., Freeman K. C., Lee Y. S., Munn J. A., Re Fiorentin P., Sivarani T., Wilhelm R., Yanny B., York D. G., 2011, ArXiv e-prints
Bland-Hawthorn J., Freeman K. C., 2003, in E. Perez, R. M. Gonzalez Delgado, & G. Tenorio-Tagle ed., Star Formation Through Time Vol. 297 of Astronomical Society of the Pacific Conference Series, Unravelling the Epoch of Dissipation. pp 457–+
Boylan-Kolchin M., Springel V., White S. D. M., Jenkins A., Lemson G., 2009, MNRAS, 398, 1150
Brook C. B., Governato F., Roškar R., Stinson G., Brooks A. M., Wadsley J., Quinn T., Gibson B. K., Snaith O., Pilkington K., House E., Pontzen A., 2011, MNRAS, 415, 1051
Brook C. B., Kawata D., Scannapieco E., Martel H., Gibson B. K., 2007, ApJ, 661, 10
Carollo D., Beers T. C., Lee Y. S., Chiba M., Norris J. E., Wilhelm R., Sivarani T., Marsteller B., Munn J. A., Bailer-Jones C. A. L., Fiorentin P. R., York D. G., 2007, Nature, 450, 1020
Chiappini C., Matteucci F., Gratton R., 1997, ApJ, 477, 765
Cooper A. P., Cole S., Frenk C. S., White S. D. M., Helly J., Benson A. J., De Lucia G., Helmi A., Jenkins A., Navarro J. F., Springel V., Wang J., 2010, MNRAS, 406, 744

De Rossi M. E., Tissera P. B., Pedrosa S. E., 2010, ArXiv e-prints
Di Matteo P., Pipino A., Lehnert M. D., Combes F., Semelin B., 2009, A&A, 499, 427
Governato F., Brook C. B., Brooks A. M., Mayer L., Willman B., Jonsson P., Stilp A. M., Pope L., Christensen C., Wadsley J., Quinn T., 2009, MNRAS, 398, 312
Governato F., Willman B., Mayer L., Brooks A., Stinson G., Valenzuela O., Wadsley J., Quinn T., 2007, MNRAS, 374, 1479
Guedes J., Callegari S., Madau P., Mayer L., 2011, ArXiv e-prints
Helmi A., Irwin M. J., Tolstoy E., Battaglia G., Hill V., Jablonka P., Venn K., Shetrone M., Letarte B., Arimoto N., Abel T., Francois P., Kaufer A., Primas F., Sadakane K., Szeifert T., 2006, ApJ, 651, L121
Huang S., Carlberg R. G., 1997, ApJ, 480, 503
Johnston K. V., Bullock J. S., Sharma S., Font A., Robertson B. E., Leitner S. N., 2008, ApJ, 689, 936
Kawata D., Gibson B. K., 2003, MNRAS, 340, 908
Kirby E. N., Guhathakurta P., Bolte M., Sneden C., Geha M. C., 2009, ApJ, 705, 328
Kirby E. N., Simon J. D., Geha M., Guhathakurta P., Frebel A., 2008, ApJ, 685, L43
Kobayashi C., Springel V., White S. D. M., 2007, MNRAS, 376, 1465
Lia C., Portinari L., Carraro G., 2002, MNRAS, 330, 821
Martínez-Serrano F. J., Serna A., Domínguez-Tenreiro R., Mollá M., 2008, MNRAS, 388, 39
Matteucci F., Greggio L., 1986, A&A, 154, 279
Mihos J. C., Hernquist L., 1996, ApJ, 464, 641
Mo H., van den Bosch F. C., White S., 2010, Galaxy Formation and Evolution
Mollá M., Ferrini F., 1995, ApJ, 454, 726
Mosconi M. B., Tissera P. B., Lambas D. G., Cora S. A., 2001, MNRAS, 325, 34
Nissen P. E., Schuster W. J., 2010, A&A, 511, L10+
Norris J. E., Gilmore G., Wyse R. F. G., Wilkinson M. I., Belokurov V., Evans N. W., Zucker D. B., 2008, ApJ, 689, L113
Norris J. E., Yong D., Gilmore G., Wyse R. F. G., 2010, ApJ, 711, 350
Perez M. J., Tissera P. B., Scannapieco C., Lambas D. G., de Rossi M. E., 2006, A&A, 459, 361
Rahimi A., Kawata D., Brook C. B., Gibson B. K., 2010, MNRAS, 401, 1826
Raiteri C. M., Villata M., Navarro J. F., 1996, A&A, 315, 105
Rupke D. S. N., Kewley L. J., Chien L., 2010, ArXiv e-prints
Sawala T., Guo Q., Scannapieco C., Jenkins A., White S., 2011, MNRAS, pp 64–+
Sawala T., Scannapieco C., Maio U., White S., 2010, MNRAS, 402, 1599
Scannapieco C., Gadotti D. A., Jonsson P., White S. D. M., 2010, MNRAS, 407, L41
Scannapieco C., Tissera P. B., White S. D. M., Springel V., 2005, MNRAS, 364, 552
Scannapieco C., Tissera P. B., White S. D. M., Springel V., 2006, MNRAS, 371, 1125
Scannapieco C., Tissera P. B., White S. D. M., Springel V., 2008, MNRAS, 389, 1137
Scannapieco C., White S. D. M., Springel V., Tissera P. B., 2009, MNRAS, 396, 696
Scannapieco C., White S. D. M., Springel V., Tissera P. B., 2011, ArXiv e-prints
Schaye J., Dalla Vecchia C., Booth C. M., Wiersma R. P. C., Theuns T., Haas M. R., Bertone S., Duffy A. R., McCarthy I. G., van de Voort F., 2010, MNRAS, 402, 1536
Shetrone M. D., Côté P., Sargent W. L. W., 2001, ApJ, 548, 592
Sijacki D., Springel V., Di Matteo T., Hernquist L., 2007, MNRAS, 380, 877
Springel V., 2005, MNRAS, 364, 1105
Springel V., Wang J., Vogelsberger M., Ludlow A., Jenkins A., Helmi A., Navarro J. F., Frenk C. S., White S. D. M., 2008, MNRAS, 391, 1685
Starkenburg E., Hill V., Tolstoy E., González Hernández J. I., Irwin M., Helmi A., Battaglia G., Jablonka P., Tafelmeyer M., Shetrone M., Venn K., de Boer T., 2010, A&A, 513, A34+
Stinson G., Seth A., Katz N., Wadsley J., Governato F., Quinn T., 2006, MNRAS, 373, 1074
Thielemann F., Nomoto K., Hashimoto M., 1993, in N. Prantzos, E. Vangioni-Flam, & M. Casse ed., Origin and Evolution of the Elements Explosive nucleosynthesis in supernovae.. pp 297–309
Tinsley B. M., Larson R. B., 1979, MNRAS, 186, 503
Tissera P. B., 2000, ApJ, 534, 636
Tissera P. B., White S. D. M., Pedrosa S., Scannapieco C., 2010, MNRAS, 406, 922
Tolstoy E., Venn K. A., Shetrone M., Primas F., Hill V., Kaufer A., Szeifert T., 2003, AJ, 125, 707
Venn K. A., Irwin M., Shetrone M. D., Tout C. A., Hill V., Tolstoy E., 2004, AJ, 128, 1177
Wiersma R. P. C., Schaye J., Theuns T., Dalla Vecchia C., Tornatore L., 2009, MNRAS, 399, 574
Woosley S. E., Weaver T. A., 1995, ApJS, 101, 181
Wyse R. F. G., 2010, Astronomische Nachrichten, 331, 526
Zoccali M., Hill V., Lecureur A., Barbuy B., Renzini A., Minniti D., Gómez A., Ortolani S., 2008, Astronomy & Astrophysics, 486, 177
Zolotov A., Willman B., Brooks A. M., Governato F., Brook C. B., Hogg D. W., Quinn T., Stinson G., 2009, ApJ, 702, 1058
Zolotov A., Willman B., Brooks A. M., Governato F., Hogg D. W., Shen S., Wadsley J., 2010, ApJ, 721, 738